

Article

# Direct Measure of the Local Concentration of Pyrenyl Groups in Pyrene-Labeled Dendrons Derived from the Rate of Fluorescence Collisional Quenching

Janine L. Thoma <sup>1</sup>, Stuart A. McNelles <sup>2</sup>, Alex Adronov <sup>2</sup> and Jean Duhamel <sup>1,\*</sup>

<sup>1</sup> Department of Chemistry, Institute for Polymer Research, Waterloo Institute for Nanotechnology, University of Waterloo, Waterloo, ON N2L 3G1, Canada; janine.lydia.thoma@uwaterloo.ca

<sup>2</sup> Department of Chemistry and Chemical Biology, Brockhouse Institute for Materials Research, McMaster University, 1280 Main St. W., Hamilton, ON L8S 4M1, Canada; mcnelisa@mcmaster.ca (S.A.M.); adronov@mcmaster.ca (A.A.)

\* Correspondence: jduhamel@uwaterloo.ca

Received: 13 November 2020; Accepted: 30 November 2020; Published: 5 December 2020



**Abstract:** The model-free analysis (MFA) was applied to measure the average rate constant ( $\langle k \rangle$ ) for pyrene excimer formation (PEF) in a series of pyrene-labeled dendrons referred to as  $\text{Py}_x\text{-G}(N)$ , where  $x (= 2^N)$  is the number of pyrenyl labels born by a dendron of generation  $N$  ranging from 1 to 6.  $\langle k \rangle$  was measured in four different solvents, namely tetrahydrofuran (THF), toluene,  $N,N$ -dimethylformamide (DMF), and dimethylsulfoxide (DMSO).  $\langle k \rangle$  was found to increase linearly with increasing local pyrene concentration ( $[\text{Py}]_{\text{loc}}$ ), where  $[\text{Py}]_{\text{loc}}$  had been determined mathematically for the  $\text{Py}_x\text{-G}(N)$  dendrons. The slope of each straight line changed with the nature of the solvent and represented  $k_{\text{diff}}$ , the bimolecular rate constant for PEF.  $k_{\text{diff}}$  depended on the solvent viscosity ( $\eta$ ) and the probability ( $p$ ) for PEF upon encounter between an excited and a ground-state pyrene. In a same solvent,  $k_{\text{diff}}$  for the  $\text{Py}_x\text{-G}(N)$  dendrons was about  $360 \pm 30$  times smaller than  $k_{\text{diff}}$  obtained for ethyl 4-(1-pyrene)butyrate (PyBE), a pyrene model compound similar to the pyrene derivative used to label the dendrons. The massive decrease in  $k_{\text{diff}}$  observed for the  $\text{Py}_x\text{-G}(N)$  samples reflected the massive loss in mobility experienced by the pyrenyl labels after being covalently attached onto a macromolecule compared to freely diffusing PyBE. Interestingly, the  $k_{\text{diff}}$  values obtained for the  $\text{Py}_x\text{-G}(N)$  dendrons and the PyBE model compound followed similar trends as a function of solvent, indicating that the difference in behavior between the  $k_{\text{diff}}$  values obtained in different solvents were merely due to the changes in the  $\eta$  and  $p$  values between the solvents. Normalizing the  $\langle k \rangle$  values obtained with the  $\text{Py}_x\text{-G}(N)$  dendrons by the  $k_{\text{diff}}$  values obtained for PyBE in the same solvents accounted for changes in  $\eta$  and  $p$ , resulting in a master curve upon plotting  $\langle k \rangle / (f_{\text{diff}} \times k_{\text{diff}})$  as a function of  $[\text{Py}]_{\text{loc}}$ , where  $f_{\text{diff}}$  was introduced to account for some pyrene aggregation in the higher generation dendron ( $\text{Py}_{64}\text{-G}(6)$ ). This result demonstrates that  $\langle k \rangle$  represents a direct measure of  $[\text{Py}]_{\text{loc}}$  in pyrene-labeled macromolecules.

**Keywords:** pyrene excimer fluorescence; pyrene-labeled dendrimers; model-free analysis

## 1. Introduction

Techniques such as viscometry, light scattering (LS), and small angle X-ray (SAXS) or neutron (SANS) scattering have traditionally played a critical role in the characterization of macromolecules due to their ability to determine the internal density of macromolecules in solution. Since the internal density of a macromolecule can be related to its volume after the molecular weight has been determined, such measurements provide a means to assess the dimensions of macromolecules in solution. For instance, the existence of excluded volume experienced by macromolecules in solution is readily

detected by a marked decrease in the internal density of macromolecules, which can be mathematically predicted and experimentally confirmed through intrinsic viscosity ( $[\eta]$ ) and LS measurements [1]. These measurements are typically conducted with polymer concentrations in the 1–10 g/L range, a concentration range that is suitable for well-soluble samples, but that can lead to aggregation and challenging data analysis for less soluble macromolecules.

In contrast, fluorescence is better known for its ability to probe fast photochemical processes, which has led to the implementation of many fluorescence-based applications to characterize the internal dynamics of macromolecules in solution [2]. In a typical fluorescence collisional quenching (FCQ) experiment, where quenching occurs solely upon contact between the excited dye and its quencher, a macromolecule is covalently labeled with a dye and its quencher at two specific positions, followed by the acquisition of the monoexponential fluorescence decay of the fluorescently labeled macromolecule. Analysis of the decay yields the decay time ( $\tau$ ) corresponding to the quenching of the dye by the quencher, which is equal to  $(1/\tau_o + k_{\text{diff}} \times [Q]_{\text{loc}})^{-1}$ , where  $\tau_o$ ,  $k_{\text{diff}}$ , and  $[Q]_{\text{loc}}$  are the dye natural lifetime, the bimolecular quenching rate constant describing the diffusive encounters between the excited dye and the quencher, and the quencher concentration experienced locally by the excited dye, respectively. Because  $[Q]_{\text{loc}}$  is deemed impossible to measure experimentally, the fluorescence decay analysis yields the product  $k_{\text{diff}} \times [Q]_{\text{loc}}$ , which is referred to as the pseudo-unimolecular rate constant  $k$ . Information about the internal dynamics of the macromolecule is retrieved from  $k$ , a larger  $k$  reflecting a more flexible macromolecule. Yet, this interpretation of  $k$  overlooks the fact that  $k$  is not only a function of  $k_{\text{diff}}$  but also of  $[Q]_{\text{loc}}$ , which is related to the internal density of the macromolecule, since the quencher is covalently attached to the macromolecule.

The difficulty in establishing the relationship between  $k$  and  $[Q]_{\text{loc}}$  for fluorescently labeled macromolecules is rooted in a number of technical and theoretical hurdles that must be overcome, as described in an earlier review [3]. First, most photophysical processes like FCQ occur over short distances of less than 5 nm [3]. This constraint requires that the dye and quencher be relatively close to each other, limiting the application of FCQ experiments to oligomers, not macromolecules. To study macromolecules by FCQ and resolve this first hurdle, the dye and quencher must be brought closer to each other, typically by increasing the number of dyes and quenchers attached to the macromolecule. Unfortunately, this practice leads to the second hurdle of FCQ experiments, whereby each polymer segment spanning a dye and a quencher results in a different quenching rate constant, which leads to a complex distribution of quenching rate constant ( $k_i$ ) [3]. In turn, the fluorescence decay of the randomly labeled macromolecules turns into a sum of exponentials associated with a distribution of decay times  $\tau_i$  equal to  $(1/\tau_o + k_i)^{-1}$ . Since no multiexponential decay analysis can resolve all the  $\tau_i$  values resulting from the distribution of the  $k_i$  rate constants, the average rate constant for quenching  $\langle k \rangle$  is typically determined. The relationship between  $\langle k \rangle$  and  $[Q]_{\text{loc}}$  now needs to be established, and this represents the third hurdle in FCQ experiments because  $[Q]_{\text{loc}}$  is difficult to predict for a macromolecule labeled with more than one dye and one quencher [3].

For reasons that have been presented in several reviews [3–5], excimer formation upon encounter between an excited and a ground-state pyrenyl group covalently attached onto a macromolecule is a well-known and often used FCQ application to probe the internal dynamics of macromolecules. The multiexponential fluorescence decays acquired with macromolecules labeled with more than two pyrenes can be satisfyingly fit according to the model-free analysis (MFA), which yields the average rate constant  $\langle k \rangle$  of pyrene excimer formation (PEF) [3,6]. In this case, the ground-state pyrenes act as quenchers, and  $\langle k \rangle$  is related to the local pyrene concentration ( $[Py]_{\text{loc}}$ ) experienced by an excited pyrene according to Equation (1). Equation (1) is well accepted in the literature because it has been shown to hold for homogeneous pyrene solutions [7], it agrees with the results obtained with end-labeled monodisperse polymers [8,9], and it has been predicted for polymers randomly labeled with pyrenes [10]. The MFA has been shown to be a superior analytical tool [11] compared to other procedures that have been applied previously to study the fluorescence of pyrene-labeled dendrimers [12–28], as was reported in an earlier review [4]. Yet, validation of Equation (1) is essential

to demonstrate that FCQ experiments such as those based on PEF yield parameters that report on  $[Py]_{loc}$ , and thus on the internal density of the macromolecule onto which the pyrenyl labels are attached.

$$\langle k \rangle = k_{diff} \times [Py]_{loc} \quad (1)$$

The only study to have indicated that Equation (1) is valid was conducted in tetrahydrofuran (THF) with a series of pyrene labeled dendrons referred to as  $Py_x-G(N)$ . The  $Py_x-G(N)$  dendrons were prepared with a 2,2-bis(hydroxymethyl) propionic acid backbone, the generation number ( $N$ ) of the dendrons ranged from 1 to 6, and  $x (= 2^N)$  represented the number of pyrenyl labels covalently attached to the terminal ends of a dendron of generation  $N$  [29]. The published derivation of the average squared end-to-end distance,  $\langle L_{Py}^2 \rangle^{1/2}$ , of the highly branched  $Py_x-G(N)$  dendrons was employed to estimate  $[Py]_{loc}$  for each  $Py_x-G(N)$  dendron. The MFA of the fluorescence decays acquired with the  $Py_x-G(N)$  dendrons yielded  $\langle k \rangle$ , which was found to increase linearly with increasing  $[Py]_{loc}$  as predicted by Equation (1). This original study is now extended to the three additional solvents toluene,  $N,N$ -dimethylformamide (DMF), and dimethylsulfoxide (DMSO), which provide, after including THF, a series of four solvents with a broad range of polarity and viscosity. In turn, polarity and viscosity affected the probability ( $p$ ) of forming an excimer and the diffusion coefficient ( $D$ ) of the pyrene labels in different manner, which affected the results obtained by PEF. Fortunately, these effects could be accounted for by studying PEF with homogeneous solutions of ethyl 4-(1-pyrene)butyrate (PyBE) in the same solvents, which provided a means to assess how  $k_{diff}$  in Equation (1) was affected by solvent polarity and viscosity. After accounting for the changes in  $k_{diff}$  due to solvent polarity and viscosity, all  $\langle k \rangle$  vs.  $[Py]_{loc}$  plots obtained for the  $Py_x-G(N)$  samples in the different solvents merged into a single master curve, thus demonstrating the validity and generality of Equation (1).

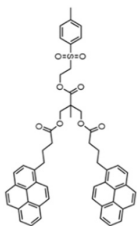
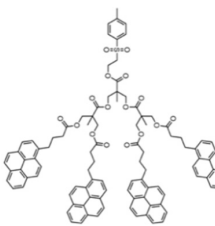
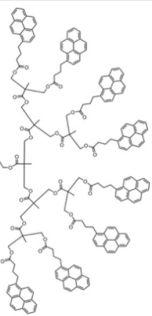
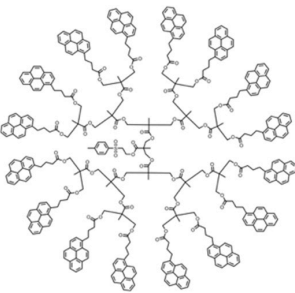
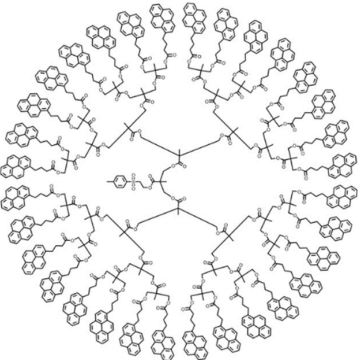
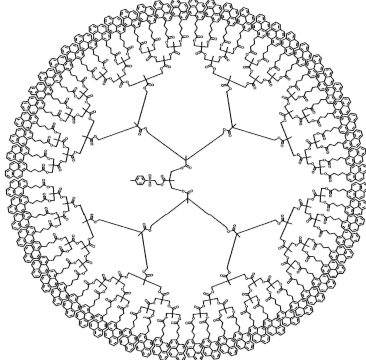
## 2. Materials and Methods

### 2.1. Materials

The six 2,2-bis(hydroxymethyl)propionic acid backbone dendrimers bearing pyrenyl labels at each terminal end have been previously synthesized, and their synthesis and characterization in THF can be reviewed in a previous publication [29]. The chemical structure of the pyrene-labeled dendrons ( $Py_x-G(N)$ ) used in this study is provided in Table 1.

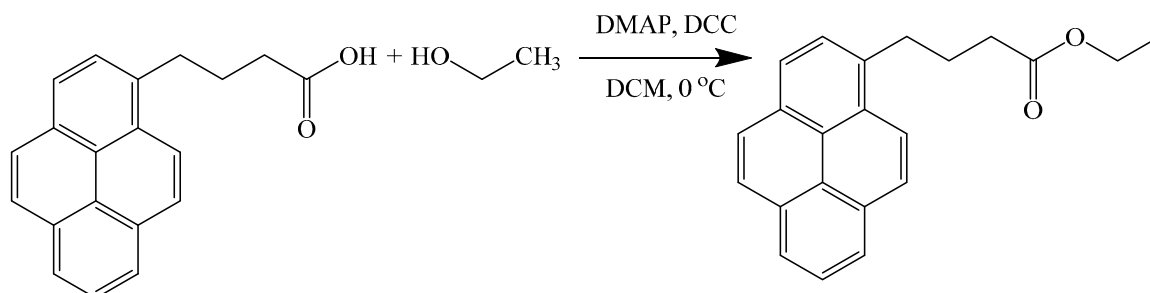
Dichloromethane (DCM,  $\geq 99.8\%$ ),  $N,N'$ -dicyclohexylcarbodiimide (DCC,  $\geq 99.0\%$ ), 4-(dimethylamino) pyridine (DMAP,  $\geq 99\%$ ),  $N,N$ -dimethylformamide (DMF,  $\geq 99.8\%$ ), dimethylsulfoxide (DMSO,  $\geq 99.9\%$ ), ethanol (reagent grade), 1-pyrenebutyric acid (97%), sodium hydroxide ( $\geq 97.0\%$ ), and sodium sulfate (anhydrous  $\geq 99.0\%$ ) were obtained from Sigma (Markham, ON, Canada). Sodium bicarbonate ( $\geq 99.7\%$ ), tetrahydrofuran optima ( $\geq 99.9\%$ ), and toluene (distilled in glass) were supplied by VWR (Mississauga, ON, Canada), Fisher Scientific (Ottawa, ON, Canada), and Caledon Laboratories (Halton Hills, ON, Canada), respectively. All chemicals were used as received.

**Table 1.** Chemical structure and  $[Py]_{loc}$  for each  $Py_x-G(N)$  dendron [29].

Sample	$Py_2-G(1)$	$Py_4-G(2)$	$Py_8-G(3)$	$Py_{16}-G(4)$
Structure				
$[Py]_{loc}$ (M)	34	62	94	140
Sample	$Py_{32}-G(5)$		$Py_{64}-G(6)$	
Structure				
$[Py]_{loc}$ (M)	212		330	

## 2.2. Synthesis of Ethyl 4-(1-pyrene)butyrate (PyBE)

The synthesis of the model compound ethyl 4-(1-pyrene)butyrate (PyBE) follows the reaction scheme outlined in Scheme 1 and is described in more detail hereafter. Freshly distilled DCM (25 mL) was added to a 50 mL round bottom flask (RBF) equipped with a magnetic stir bar. 1-Pyrenebutyric acid (1.00 g, 3.5 mmol), ethanol (1.60 g, 34.7 mmol), and DMAP (0.08 g, 0.7 mmol) were added to the RBF. The RBF was then placed in an ice water bath under a gentle flow of nitrogen (Praxair, 4.0). DCC (0.72 g, 3.5 mmol) was dissolved in 5 mL of DCM, and the solution was added dropwise to the RBF over 30 min. The reaction was left stirring under a nitrogen atmosphere at room temperature for 18 h. The next day, the reaction solution was filtered using suction filtration to remove the urea precipitate. The reaction solution was then washed with 0.5 M HCl, a saturated solution of sodium bicarbonate, and a saturated solution of sodium chloride. The organic layer was extracted after each wash and dried with sodium sulfate. Silica gel chromatography was then used to purify PyBE using a 1:10 ethyl acetate:hexane mixture. The final product was isolated as a colourless solid and dried in vacuo overnight (0.68 g, 62%). The  $^1H$  NMR spectrum is shown in Figure S1 in the Supplementary Materials (SM), and its molar absorbance coefficient at 344 nm equals  $42,600 \pm 140 M^{-1} \cdot cm^{-1}$  in THF.



**Scheme 1.** Chemical reaction scheme of the synthesis of the model compound ethyl 4-(1-pyrene) butyrate (PyBE).

### 2.3. UV-Vis Spectroscopy

All absorption measurements were carried out on a Varian Cary 100 Bio spectrophotometer (Varian, Palo Alto, CA, USA). The Py(*x*)-G(*N*) solutions were prepared with a pyrene concentration of  $2.5 \times 10^{-6}$  M equivalent to an optical density of 0.1. The absorbance measurements were made using a quartz cuvette with a 10 mm path length.

### 2.4. Steady-State Fluorometer

All steady-state fluorescence (SSF) measurements were performed on a QM-400 spectrofluorometer equipped with a Xenon arc lamp (HORIBA, London, ON, Canada). The different pyrene solutions in organic solvents were degassed for 30–45 min depending on the organic solvent. and their spectra were acquired with a 344 nm excitation wavelength and over wavelengths ranging from 350 to 600 nm. The SSF measurements with the Py<sub>*x*</sub>-G(*N*) dendrons were conducted using the conventional right-angle geometry, and the measurements carried out with more concentrated solutions of the PyBE model compound were performed using the front face geometry to avoid the inner filter effect and reabsorption. The intensity of the excimer emission,  $I_E$ , was divided by the intensity of the monomer emission,  $I_M$ , to obtain the  $I_E/I_M$  ratio, which is a measure of PEF efficiency.  $I_M$  was calculated by integrating the area under the first fluorescence peak of the monomer fluorescence spectrum from  $\lambda_{0-0} - 4$  nm to  $\lambda_{0-0} + 4$  nm, where  $\lambda_{0-0}$  corresponds to the wavelength of the 0-0 transition of the pyrene derivative in a given solvent. Since  $I_E$  was much less sensitive to solvent differences, it was calculated by integrating the excimer fluorescence intensity under the spectrum from 500 to 530 nm.

### 2.5. Time-Resolved Fluorometer

A FluoroHub fluorometer (HORIBA, Piscataway, NJ, USA) equipped with a DeltaDiode at 336 nm was used to acquire the monomer and excimer time-resolved fluorescence (TRF) decays of the degassed solutions of the Py<sub>*x*</sub>-G(*N*) dendrons and PyBE in the different solvents at 375 and 510 nm with a 370 and 490 nm cut off filter, respectively. The cut off filters prevented stray light from reaching the fluorescence detector. All decays had 20,000 counts at their maximum and were acquired over 1024 channels with times-per-channel of 0.435, 0.0514 or 0.102 ns/ch. A 2.04 ns/ch time-per-channel was used for the fluorescence decays of  $2.5 \times 10^{-6}$  M dilute solutions of the PyBE and Py<sub>1</sub>-G(0) model compounds acquired to determine the natural lifetime ( $\tau_M$ ) of the pyrene derivatives. The instrument response function (IRF) was obtained with an aluminum reflective monolith by setting the emission wavelength at 336 nm. The IRF was then convoluted with the mathematical expressions for the time-dependent concentration of the pyrene monomer and excimer given in SI as Equations (S1) and (S2) for the MFA [3,6] and as Equations (S3) and (S4) for the Birks scheme analysis [7,9]. The parameters in Equations (S1)–(S4) were optimized according to the Marquardt–Levenberg algorithm [30]. The quality of the fits was gauged from a low  $\chi^2$  ( $< 1.20$ ) and residuals and autocorrelation of the residuals randomly distributed around zero.

## 2.6. Model-Free Analysis (MFA) of the Fluorescence Decays

The model-free analysis (MFA) is a global analysis tool which can be used to simultaneously fit a monomer and excimer decay [3–6,29]. The MFA can be used to fit the decays of any molecule or macromolecule labeled with the chromophore pyrene. When pyrene becomes excited by a photon of light, it can decay to the ground state using one of two pathways. It can either fluoresce with its monomeric lifetime,  $\tau_M$ , or it can encounter another ground-state pyrene and form one of two excimers. An excimer can be the result of the proper (E0) and improper (D) stacking of two pyrenyl groups and they have their own lifetime,  $\tau_{E0}$  and  $\tau_D$ , respectively. Three different pyrene species are expected to co-exist in solution, namely those pyrenes that are isolated in solution and cannot form excimer ( $Py_{free}^*$ ), form an excimer through diffusive encounters ( $Py_{diff}^*$ ), and are pre-aggregated ( $E0^*$  or  $D^*$ ). The MFA yields the molar fractions  $f_{free}$ ,  $f_{diff}$ , and  $f_{agg}$  ( $= f_{E0} + f_D$ ) of the pyrene species  $Py_{free}^*$ ,  $Py_{diff}^*$ ,  $E0^*$ , and  $D^*$ , respectively. In some instances, a contribution from residual scattering or possibly short-lived pyrene dimers is seen in the excimer decays, and an exponential with a short lifetime ( $\tau_S$ ) of 4 ns is added to the expression of the excimer decay during the decay analysis. More information about the details of the MFA can be found as SM, along with the equations used to fit the pyrene monomer and excimer fluorescence decays.

Using the decay times,  $\tau_i$ , and pre-exponential factors,  $a_i$ , calculated by the MFA, the average lifetime,  $\langle \tau \rangle$ , as well as the average rate constant of excimer formation,  $\langle k \rangle$ , can be calculated as shown using Equations (2) and (3), respectively.

$$\langle \tau \rangle = \sum_{i=1}^3 a_i \tau_i \quad (2)$$

$$\langle k \rangle = \frac{1}{\langle \tau \rangle} - \frac{1}{\tau_M} \quad (3)$$

Using the molar fractions of the different pyrene species along with  $\langle \tau \rangle$  and  $\langle k \rangle$ , the  $I_E/I_M^{TRF}$  ratio representing the absolute  $I_E/I_M$  ratio shown in Equation (4) can be calculated [31].

$$I_E/I_M^{TRF} = \frac{(f_{diff} f_{E0} \tau_{E0} + f_{diff} f_D \tau_D) \langle \tau \rangle \langle k \rangle + f_{E0} \tau_{E0} + f_D \tau_D}{f_{diff} \langle \tau \rangle + f_{free} \tau_M} \quad (4)$$

## 2.7. Birks Scheme Analysis of the Fluorescence Decays

The pyrene monomer and excimer fluorescence decays of PyBE were also fitted globally with Equations (S3) and (S4), respectively. In this case, the excimer is assumed to be produced by diffusive encounters between an excited and a ground-state pyrene label with a single rate constant  $k_{diff}$ . The excimer can then fluoresce with its natural lifetime  $\tau_{E0}$  or dissociate by returning an excited and ground-state pyrene with a dissociation rate constant  $k_{-1}$ . Global analysis of the decays yields  $k_{diff} \times [PyBE]$ ,  $k_{-1}$ , and  $\tau_{E0}$ , where  $[PyBE]$  is the concentration of the PyBE model compound [7,9,32].

## 3. Results and Discussion

The average squared end-to-end distance,  $\langle L_{Py}^2 \rangle^{1/2}$ , of a series of 2,2-bis(hydroxymethyl)propionic acid backbone dendrons labeled with 1-pyrenebutyric acid at their terminal ends ( $Py_x-G(N)$ ) is shown in Equation (5), which has been derived in an earlier publication [29]. The parameters  $a$  ( $= 6$ ) and  $b$  ( $= 8$ ) in Equation (5) represent the number of atoms connecting the pyrene label to the first junction point and the number of atoms resulting from the incorporation of each bis(hydroxymethyl)propionic acid in the construct, respectively. In Equation (5),  $l$  represents the projection of a C–C bond length taken to equal 0.125 nm.

$$\langle L_{Py}^2 \rangle = l^2 \left( 1 + 2a + b \frac{N \times 2^N - 2^{N+1} + 2}{2^N - 1} \right) \quad (5)$$

$[Py]_{loc}$  could then be determined with Equation (6), where  $N_A$  is the Avogadro number and the term  $(2^N - 1)$  represents the number of ground-state pyrenes in the  $Py_x-G(N)$  dendron after considering that one pyrenyl label must be excited in a PEF experiment. The  $[Py]_{loc}$  concentrations corresponding to the different  $Py_x-G(N)$  dendrons are provided in Table 1. The very large  $[Py]_{loc}$  concentrations reported in Table 1 are a result of the short distances separating the ends of the dendrons in comparison to their overall size. For instance, a linear chain made of 16 bonds would have an end-to-end distance equal to  $16^{0.5} \times l = 0.5$  nm using an  $l$  value of 0.125 nm. This end-to-end distance would result in a molar concentration for one chain end according to Equation (6) equal to 44 M, which is much larger than many organic solvents, but is a consequence of dealing with the end-to-end distance of a molecule instead of its overall size that is much larger. With their much higher number of chain ends, the  $Py_x-G(N)$  dendrons have considerably higher local concentrations of chain ends, as reported in Table 1.

$$[Py]_{loc} = \frac{4}{3}\pi \frac{2^N - 1}{(\langle L_{Py}^2 \rangle^{1/2} / 2)^3 \times N_A} \quad (6)$$

The steady-state fluorescence (SSF) spectra for each  $Py_x-G(N)$  sample were acquired in the different solvents and are shown in Figure 1 for toluene, DMF, and DMSO.  $Py_2-G(1)$ , which contains two pyrenyl groups, produces the least amount of excimer in each solvent, and PEF was found to increase with generation number and the number of pyrenyl groups present in a given  $Py_x-G(N)$  dendron, thus reflecting a direct relationship between the PEF efficiency and  $[Py]_{loc}$ . The SSF spectra shown in Figure 1 are typical of a pyrene-labeled macromolecule, and the PEF efficiency can be better quantified by considering the  $I_E/I_M$  ratio, which is proportional to  $k_{diff}$  and  $[Py]_{loc}$ , as shown in Equation (7). The expression of  $k_{diff}$  is given in Equation (8), where  $R$ ,  $D$ , and  $p$  are the molecular diameter of pyrene, twice the diffusion coefficient of pyrene, and the probability of having PEF upon a diffusive encounter between an excited and a ground-state pyrene, respectively [2]. The expression of the diffusion coefficient ( $D_{Py}$ ) for one pyrene molecule is given in Equation (9), where  $k_B$ ,  $T$ ,  $\eta$ , and  $R_h$  are the Boltzmann constant, the absolute temperature, the solvent viscosity, and the hydrodynamic radius of the dye, respectively. Based on Equations (7)–(9),  $k_{diff}$ , and thus the  $I_E/I_M$  ratio, is proportional to the ratio  $p/\eta$ , which depends critically on the dielectric constant (reported at 20 °C) and viscosity (reported at 25 °C) of the solvent, which equal 2.4 and 0.56 mPa.s, 7.5 and 0.46 mPa.s, 38 and 0.79 mPa.s, and 47 and 1.99 mPa.s for toluene, THF, DMF, and DMSO, respectively [33].

$$\frac{I_E}{I_M} \propto k_{diff} \times [Py]_{loc} \quad (7)$$

$$k_{diff} = 4\pi N_A R D p \quad (8)$$

$$D = \frac{k_B T}{6\pi\eta R_h} \quad (9)$$

The  $I_E/I_M$  ratios of the  $Py_x-G(N)$  dendrons were plotted in Figure 2a for each solvent. The  $I_E/I_M$  ratio increased with increasing generation number. However, and as predicted by Equations (7)–(9), the  $I_E/I_M$  ratio did not depend solely on the viscosity of the solvent. For instance, toluene with a viscosity higher than THF was found to form excimer more efficiently, followed by THF, DMF, and finally DMSO. THF, which is more than four times less viscous than DMSO, yielded  $I_E/I_M$  ratios that were only 2.4-fold larger than those obtained in DMSO. This behaviour was a result of the different  $p$  values taken in Equation (8) for different solvents. The  $I_E/I_M$  ratios were also plotted as a function of  $[Py]_{loc}$  in Figure 2b. Fairly linear trends were obtained between  $I_E/I_M$  and  $[Py]_{loc}$  up to  $Py_{32}-G(5)$ , but clear deviations from linearity were observed for  $Py_{64}-G(6)$ . The linear increase in  $I_E/I_M$  with increasing  $[Py]_{loc}$  agreed with the behavior expected from Equation (7).

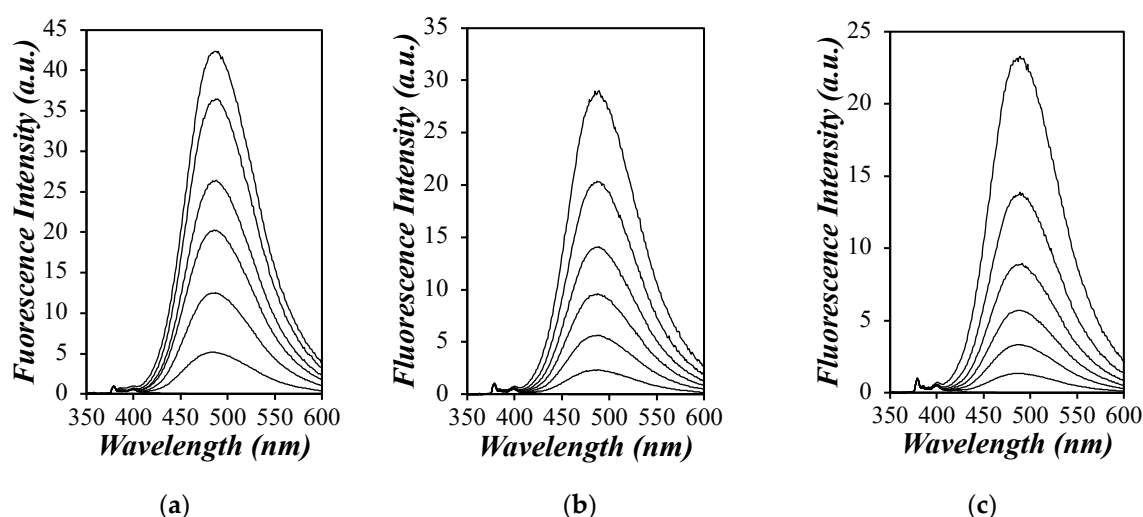


**Figure 1.** Steady-state fluorescence (SSF) spectra of the  $\text{Py}_x\text{-G}(N)$  dendrons normalized at the 0-0 transition of pyrene ( $\sim 378$  nm) in (a) toluene, (b)  $N,N$ -dimethylformamide (DMF), and (c) dimethylsulfoxide (DMSO). From top to bottom:  $\text{Py}_{64}\text{-G}(6)$ ,  $\text{Py}_{32}\text{-G}(5)$ ,  $\text{Py}_{16}\text{-G}(4)$ ,  $\text{Py}_8\text{-G}(3)$ ,  $\text{Py}_4\text{-G}(2)$ , and  $\text{Py}_2\text{-G}(1)$ .  $\lambda_{\text{ex}} = 344$  nm,  $[\text{Py}] = 2.5 \times 10^{-6}$  M.

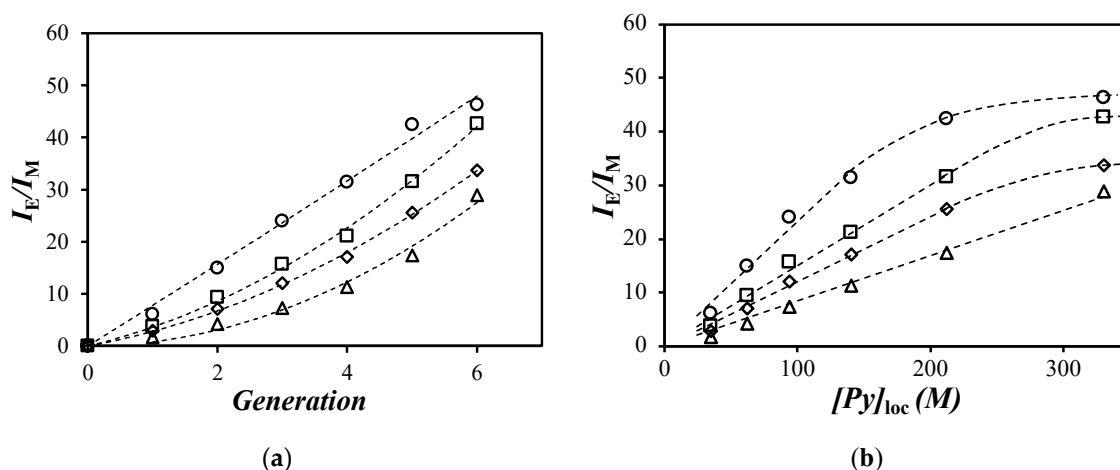


**Figure 2.** Plot of the  $I_E/I_M$  ratios for each  $\text{Py}_x\text{-G}(N)$  dendron in (●) toluene, (■) tetrahydrofuran (THF) [29], (◆) DMF, and (▲) DMSO versus (a) generation number and (b) the  $[\text{Py}]_{\text{loc}}$ .

The somewhat odd behavior observed in Figure 2b for  $\text{Py}_{64}\text{-G}(N)$ , whereby the  $I_E/I_M$  ratio is smaller than anticipated, has two most plausible causes. One would be the presence of a small but strongly emissive amount of unattached pyrenyl labels, which would artificially increase the pyrene monomer emission, thus reducing the  $I_E/I_M$  ratio as was illustrated in an earlier publication [11]. The second would be the enhanced crowding of the terminal pyrenyl groups for the  $\text{Py}_{64}\text{-G}(6)$  sample leading to a reduction in the number of pyrenyl groups available for diffusive PEF, and thus resulting in less efficient PEF as was suggested earlier for the trends obtained in THF [29]. To address these concerns as well as the somewhat erratic behavior shown in Figure 2b where each solvent yielded a different trend, a more detailed analysis of the fluorescence data is required by applying the model-free analysis (MFA) to the fluorescence decays of the  $\text{Py}_x\text{-G}(N)$  samples. The MFA dissects the PEF process into its dynamic and structural components given by the average rate constant  $\langle k \rangle$  for PEF (see Equation (1)) and the molar fractions of the different pyrene species contributing to PEF, respectively.

The TRF decays of each  $\text{Py}_x\text{-G}(N)$  dendron were acquired in toluene, DMF, and DMSO and then analysed using the model-free analysis (MFA). The global MFA of the decays gave excellent fits with a  $\chi^2 \leq 1.2$ , and residuals and autocorrelation residuals randomly distributed around zero. A sample fit



is shown in Figure S2. A detailed explanation of the MFA can be found as Supplementary Materials (SM) as well as all the parameters retrieved from the fits in Tables S3–S5. The MFA parameters were used to calculate  $\langle k \rangle$  from Equation (3) and the molar fractions of the different pyrene species. These molar fractions  $f_{\text{free}}$ ,  $f_{\text{diff}}$ , and  $f_{\text{agg}}$  represent the pyrenes that do not form excimer in solution and are usually free unattached pyrene derivatives, form excimer through diffusive encounters, and form excimer through direct excitation of a pyrene aggregate, respectively. To ensure that the parameters retrieved from the MFA provided an accurate representation of the fluorescence spectra shown in Figure 2, the parameters retrieved from the MFA of the decays were used to calculate the absolute  $I_E/I_M^{\text{TRF}}$  ratios using Equation (4). The absolute  $I_E/I_M^{\text{TRF}}$  ratios calculated from Equation (4) should be proportional to the relative  $I_E/I_M^{\text{SSF}}$  ratios obtained from the analysis of the SSF spectra. The linear relationship observed in Figure 3 between the  $I_E/I_M^{\text{TRF}}$  and  $I_E/I_M^{\text{SSF}}$  ratios demonstrated that the MFA parameters retrieved from the global analysis of the fluorescence decays agreed with the analysis of the fluorescence intensities in the fluorescence spectra. The average rate constant  $\langle k \rangle$  could now be studied in more detail.

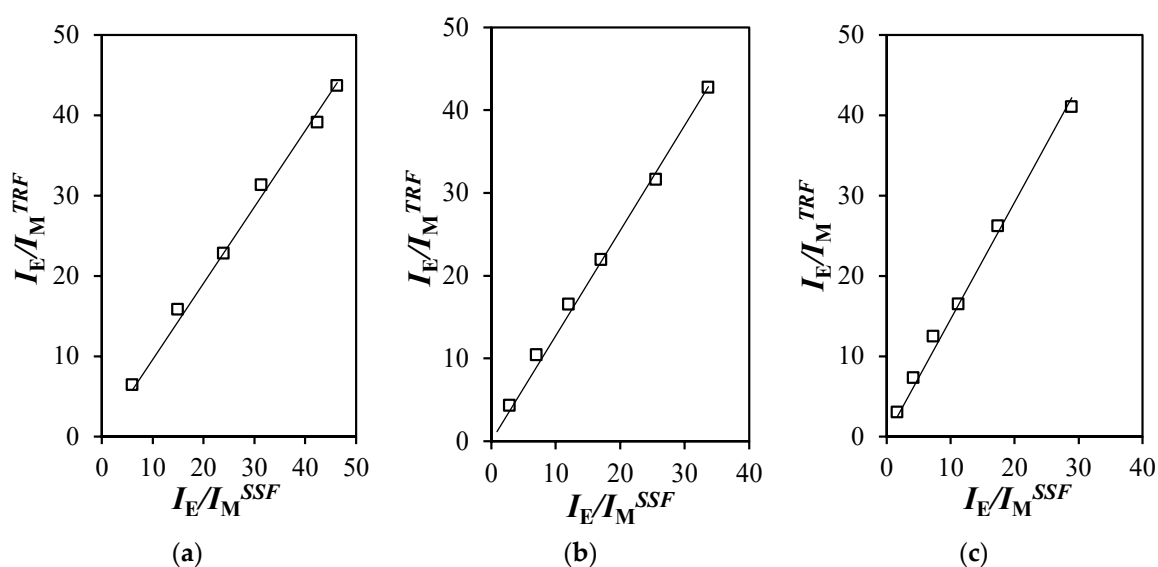


**Figure 3.** Plot of  $I_E/I_M^{\text{TRF}}$  versus  $I_E/I_M^{\text{SSF}}$  for the  $\text{Py}_x\text{-G}(N)$  samples in (a) toluene, (b) DMF, and (c) DMSO.

Figure 4a shows a plot of  $\langle k \rangle$  vs.  $[\text{Py}]_{\text{loc}}$  for the  $\text{Py}_x\text{-G}(N)$  samples in the three solvents. As for the  $I_E/I_M^{\text{SSF}}$  ratios in Figure 2b,  $\langle k \rangle$  increased linearly with increasing  $[\text{Py}]_{\text{loc}}$  for  $N$  values ranging from 1 to 5 but showed a clear downward curvature for  $\text{Py}_{64}\text{-G}(6)$ . The same behavior had been observed earlier in THF, and this behavior had been attributed to increased aggregation of the pyrenyl labels, which lowered the local concentration of active pyrenyl labels that could form excimer by diffusive encounters between an excited and a ground-state pyrene [29]. The notion that the pyrenyl labels were strongly aggregated in the  $\text{Py}_{64}\text{-G}(6)$  sample was easily illustrated by plotting the molar fraction of aggregated pyrenes ( $f_{\text{agg}}$ ) as a function of the generation number in Figure 4b. While the  $\text{Py}_x\text{-G}(N)$  samples with  $1 \leq N \leq 5$  yielded  $f_{\text{agg}}$  values that were smaller than 0.06,  $f_{\text{agg}}$  for the  $\text{Py}_{64}\text{-G}(6)$  sample took a value that was larger than 0.17 in all solvents studied. Since  $\langle k \rangle$  is unaffected by the presence of free pyrene derivatives, this result confirmed our earlier analysis [29] that the unexpected behavior observed for  $\text{Py}_{64}\text{-G}(6)$  in Figures 2b and 5a was probably a consequence of extensive aggregation of the pyrenyl labels due to overcrowding. Dividing  $\langle k \rangle$  by the molar fraction of pyrenyl groups, which form excimer exclusively through diffusive encounters ( $f_{\text{diff}}$ ) [29], accounts for this artefact by increasing  $\langle k \rangle$  to the value that it should take if all its pyrenyl groups were dissolved in the solution, as assumed by Equation (6) for the calculation of  $[\text{Py}]_{\text{loc}}$ .

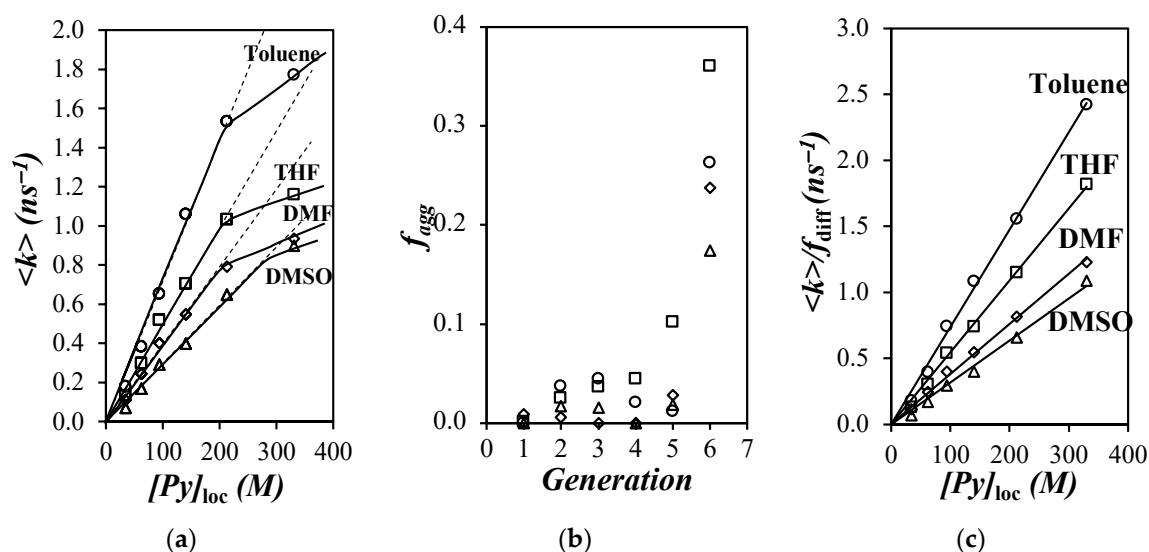


**Figure 4.** Plot of (a)  $\langle k \rangle$  versus  $[Py]_{loc}$  for the  $Py_x-G(N)$  dendrons, (b)  $f_{agg}$  calculated by the model-free analysis (MFA) for each generation, and (c)  $\langle k \rangle / f_{diff}$  versus  $[Py]_{loc}$  for the  $Py_x-G(N)$  dendrons in (●) toluene, (■) THF [29], (◇) DMF, and (▲) DMSO.

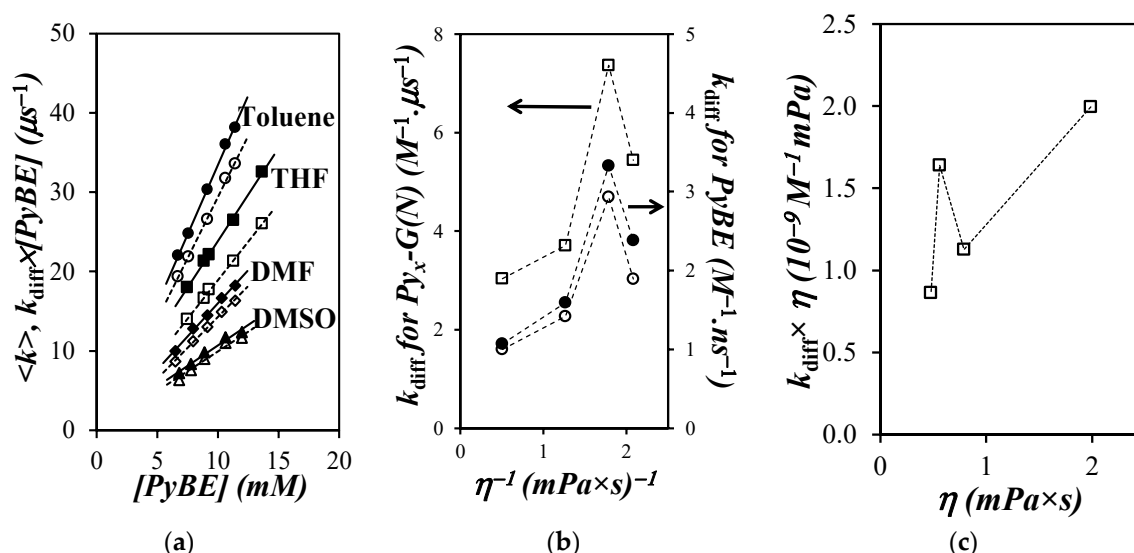


**Figure 5.** (a)  $\langle k \rangle$  and  $k_{diff} \times [PyBE]$  versus  $[PyBE]$  in (●, ●) toluene, (■, ■) THF, (◇, ◇) DMF, and (▲, ▲) DMSO; solid and hollow symbols are for the fluorescence decay analysis according to the Birks scheme and MFA, respectively. (b) Plot of  $k_{diff}$  for (■) the  $Py_x-G(N)$  dendrons and the PyBE model compound when the fluorescence decays were fitted according to (●) the MFA and (●) the Birks scheme. (c)  $k_{diff} \times \eta$  of PyBE versus solvent viscosity.

This correction was applied, and the ratio  $\langle k \rangle / f_{diff}$  was plotted as a function of  $[Py]_{loc}$  in Figure 4c. The linear relationships obtained in the plots shown in Figure 4c for all  $Py_x-G(N)$  dendrons in toluene, THF, DMF, and DMSO validated the proposal that the unexpected behavior observed for the  $I_E/I_M^{SSF}$  and  $\langle k \rangle$  parameters in Figures 2b and 5a was due to extensive aggregation of the pyrenyl groups in  $Py_{64}-G(6)$ . Similarly to the trends obtained in Figure 2b with the  $I_E/I_M^{SSF}$  ratios,  $\langle k \rangle$  was found to be larger in the more viscous toluene than in THF. In an effort to identify the origin of this phenomenon and assess whether it was general or specific to the family of  $Py_x-G(N)$  dendrons, the PEF process was investigated further with ethyl 4-(1-pyrene)butyrate (PyBE), which was used as a model compound, since it resembles the pyrene derivative covalently bound to the  $Py_x-G(N)$  samples.

The fluorescence spectra of PyBE solutions with concentrations ranging from 6 to 14 mM were acquired in toluene, THF, DMF, and DMSO and are presented in Figure S3 in SM. The fluorescence spectra showed the expected spectral features of a pyrene derivative forming excimer, with a set of sharp peaks observed between 370 and 410 nm indicative of the pyrene monomer and a broad structureless emission centered at 480 nm for the excimer. Increasing the PyBE concentration resulted in increased pyrene–pyrene encounters that resulted in increased PEF. The fluorescence spectra shown in Figure S3 were analyzed to obtain their  $I_E/I_M^{\text{SSF}}$  ratios, which were plotted as a function of the PyBE concentration in Figure S4. The plots were linear as expected for PEF, but they also displayed the same unexpected trend observed with the  $\text{Py}_x\text{-G}(N)$  dendrons that showed more viscous toluene yielding larger  $I_E/I_M^{\text{SSF}}$  ratios than less viscous THF.

The fluorescence decays of the pyrene monomer and excimer of all the PyBE solutions were acquired and analyzed according to the Birks scheme and the MFA. The parameters retrieved from the Birks scheme analysis and MFA for the PyBE solutions are listed in Tables S1 and S2, respectively. The fluorescence decay fits were excellent with the MFA in all solvents and for the Birks scheme in toluene and THF, but showed some slight deviations at the early times in DMF and DMSO, possibly due to the increased viscosity of the two latter solvents. Nevertheless, the product  $k_{\text{diff}} \times [\text{PyBE}]$  obtained from the Birks scheme analysis of the fluorescence decays and  $\langle k \rangle$  obtained from the MFA are plotted as a function of the PyBE concentration in Figure 5a. Both  $\langle k \rangle$  and  $k_{\text{diff}} \times [\text{PyBE}]$  increased linearly with increasing PyBE concentration, with  $\langle k \rangle$  being always slightly smaller than the product  $k_{\text{diff}} \times [\text{PyBE}]$ , probably a consequence of the different assumptions made for the derivation of each model. The Birks scheme assumes that the pyrene excimer dissociates with a dissociation rate constant that is typically small compared to  $1/\tau_{E0}$ , as found experimentally in Table S1, whereas the MFA neglects the excimer dissociation altogether. The Birks scheme also assumes a single rate constant for excimer formation, whereas the MFA assumes that the excimer can be formed by several rate constants. The poorer fits obtained for the fit of the fluorescence decays with the Birks scheme analysis in DMF and DMSO suggest that the MFA is a more robust analysis method. Nevertheless, the slopes of the plots of  $\langle k \rangle$  and  $k_{\text{diff}} \times [\text{PyBE}]$  as a function of PyBE concentration in Figure 5a and of  $\langle k \rangle$  versus  $[\text{Py}]_{\text{loc}}$  in Figure 4c yielded the bimolecular rate constant ( $k_{\text{diff}}$ ) for diffusive encounters between two pyrene molecules for PyBE and the pyrenyl labels of the  $\text{Py}_x\text{-G}(N)$  dendrons, respectively. They are plotted in Figure 5b as a function of the inverse of the solution viscosity.

The three plots for  $k_{\text{diff}}$  show some striking similarities with a sharp maximum for a  $1/\eta$  value of  $1.79 \text{ (mPa}\cdot\text{s)}^{-1}$  obtained in toluene. The common behavior observed for the pyrenyl labels of the  $\text{Py}_x\text{-G}(N)$  dendrons and PyBE demonstrates that this behavior is a result of the pyrene dye and not due to the fact that it is attached onto the dendrons.  $k_{\text{diff}}$  was found to be  $360 \pm 30$  times larger for the PyBE model compound than for the pyrenyl labels covalently attached to the dendrons. This massive reduction in  $k_{\text{diff}}$  reflects the equally massive loss in mobility experienced by a pyrene derivative upon covalent attachment to a macromolecule versus the same pyrene derivative freely diffusing in solution. Another important feature of Figure 5b is that  $k_{\text{diff}}$  is not inversely proportional to the solution viscosity, because PEF depends also on the probability ( $p$ ) of forming an excimer upon encounter between two pyrene moieties, as discussed in Equations (7)–(9). This aspect is further illustrated with Figure 5c, which shows the product  $\eta \times k_{\text{diff}}$ , which is proportional to  $p$ , plotted as a function of the solvent viscosity. For the four solvents investigated,  $\eta \times k_{\text{diff}}$  fluctuates from  $0.86 \times 10^9 \text{ M}^{-1}\cdot\text{mPa}$  in THF to  $2.00 \times 10^9 \text{ M}^{-1}\cdot\text{mPa}$  in DMSO. Additionally, the  $\eta \times k_{\text{diff}}$  value of  $1.13 \times 10^9 \text{ M}^{-1}\cdot\text{mPa}$  for DMF was almost half that of  $2.00 \times 10^9 \text{ M}^{-1}\cdot\text{mPa}$  in DMSO, suggesting a similar relationship for  $p$  as had been suggested earlier with two other pyrene model compounds, namely 1-pyrenemethylacetamide [34] and *n*-butyl-1-pyreneacetamide [35].

For the sake of consistency, the  $\langle k \rangle/f_{\text{diff}}$  values obtained for the  $\text{Py}_x\text{-G}(N)$  dendrons in different solvents were divided by the  $k_{\text{diff}}$  values of 1.90, 2.93, 1.42, and  $1.00 \text{ M}^{-1}\cdot\text{ns}^{-1}$  obtained from the MFA of the PyBE decays acquired in THF, toluene, DMF, and DMSO (see Figure 5b) to account for the changes in the ratio  $p/\eta$  between the different solvents. The quantity  $\langle k \rangle/(f_{\text{diff}} \times k_{\text{diff}})$  was plotted

as a function of  $[Py]_{loc}$  in Figure 6 for the four solvents considered. All data points in Figure 4c collapsed along a master line in Figure 6, indicating that this correction accounted for the different  $p/\eta$  values of the solvents. The data points showed more scatter for the higher generation dendrimers, possibly because the pyrenyl labels were more aggregated, but also because the larger dendrons might have been subject to more excluded volume effects, which are not accounted for by the derivation of Equation (4). The smaller dendrons are likelier to be devoid of solvent effects, and their behavior is well-described by Equation (4), which assumes that each chain segment behaves like a Gaussian chain. Finally, the straight line obtained between  $\langle k \rangle / (f_{diff} \times k_{diff})$  and  $[Py]_{loc}$  demonstrates that  $\langle k \rangle$  responds directly to  $[Py]_{loc}$  for the pyrene-labeled dendrons regardless of the nature of the solvent.

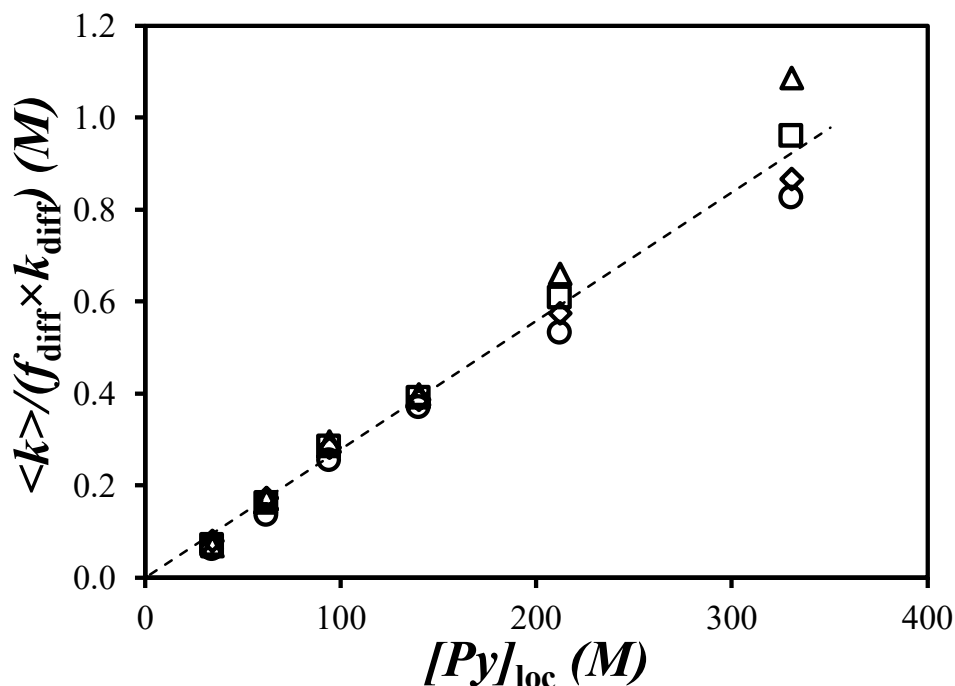


**Figure 6.** Plot of  $\langle k \rangle / (f_{diff} \times k_{diff})$  as a function of  $[Py]_{loc}$  for the  $Py_x-G(N)$  dendrons where the  $\langle k \rangle$  values obtained for the dendrimers in a given solvent are divided by  $f_{diff}$  to account for possible aggregation of the pyrenyl labels and  $k_{diff}$  obtained from the MFA of the PyBE fluorescence decays in the same solvent to account for the  $p/\eta$  term in Equations (8)–(9); (●) toluene, (■) THF [29], (◆) DME, and (▲) DMSO.

#### 4. Conclusions

A series of six pyrene end-labeled dendrons ( $Py_x-G(N)$ ) were studied in toluene, THF, DMF, and DMSO. These four solvents had different polarity and viscosity, which affected PEF through diffusive encounters between the pyrenyl labels differently. Accounting for the ratio  $p/\eta$  by dividing the  $\langle k \rangle$  values obtained for each  $Py_x-G(N)$  samples in different solvents by  $k_{diff}$  obtained for the model compound PyBE in the same solvents yielded a straight line between  $\langle k \rangle / (f_{diff} \times k_{diff})$  and  $[Py]_{loc}$ . This relationship was found to hold regardless of the nature of the solvents, particularly for the smaller dendrons that are devoid of solvent effects. It also demonstrates that  $\langle k \rangle$  obtained from the MFA of the fluorescence decays acquired with pyrene-labeled macromolecules depends directly on  $[Py]_{loc}$  and can thus be used to probe the internal density of macromolecules in the same manner as other techniques like intrinsic viscosity or static light scattering do. The main difference between PEF and these other techniques is that it takes advantage of the extreme sensitivity of fluorescence, which allows fluorescence measurements to be performed with PyLM solutions as low as 1 mg/L, two to three orders of magnitude lower than all other standard techniques that are used to characterize macromolecules in solution.

**Supplementary Materials:** The following are available online at <http://www.mdpi.com/2073-4360/12/12/2919/s1>: **Scheme S1:** Pyrene excimer formation according to the Birks scheme; **Figure S1:**  $^1\text{H-NMR}$  spectrum of ethyl 4-(1-pyrene)butyrate (PyBE). (300 MHz,  $\text{CDCl}_3$ ):  $\delta$  1.30 (t, 3H), 2.23 (p, 2H), 2.48 (t, 2H), 3.42 (t, 2H), 4.18 (q, 2H), 7.82–8.41 (m, 9H); **Figure S2:** MFA of the (A) monomer ( $\lambda_{\text{em}} = 375$  nm) and (B) excimer ( $\lambda_{\text{em}} = 510$  nm) decay of  $\text{Py}_{32}\text{-G}(5)$  in degassed DMSO.  $\chi^2 = 1.13$ ,  $\lambda_{\text{ex}} = 344$  nm; **Figure S3:** SSF spectrum of ethyl 4-pyrenylbutanoate in (A) THF, (B) toluene, (C) DMF, and (D) DMSO; **Figure S4:** Plot of the  $I_{\text{E}}/I_{\text{M}}$  ratio versus concentration of PyBE in (●) toluene, (■) THF, (◆) DMF, and (▲) DMSO; **Table S1:** Parameters retrieved from the global Birks scheme analysis of both the monomer and excimer decays of ethyl 4-(1-pyrene)butyrate in degassed toluene (Tol), *N,N*-dimethylformamide (DMF), dimethylsulfoxide (DMSO), and tetrahydrofuran (THF). Analysis program: globirks32bg; **Table S2:** Parameters retrieved from the MFA (analysis program: sumegs10bg) of both the monomer and excimer decays of ethyl 4-(1-pyrene)butyrate in degassed tetrahydrofuran (THF), degassed toluene (Tol), degassed dimethylformamide (DMF), and degassed dimethylsulfoxide (DMSO); **Table S3:** Parameters retrieved from the MFA (analysis programs: sumegs14bg or sumegs33bg-4) of the monomer decays of the  $\text{Py}_x\text{-G}(N)$  dendrons in degassed toluene (Tol), degassed dimethylformamide (DMF), and degassed dimethylsulfoxide (DMSO); **Table S4:** Parameters retrieved from the MFA of the excimer decays of the  $\text{Py}_x\text{-G}(N)$  dendrons in degassed toluene (Tol), degassed dimethylformamide (DMF), and degassed dimethylsulfoxide (DMSO); **Table S5:** Molar fractions obtained from the MFA of the  $\text{Py}_x\text{-G}(N)$  dendrons in degassed toluene (Tol), degassed dimethylformamide (DMF), and degassed dimethylsulfoxide (DMSO).

**Author Contributions:** S.A.M. synthesized all pyrene-labeled dendrimers under the supervision of A.A. J.L.T. conducted all the fluorescence experiments and analysis of the fluorescence spectra and decays, while J.D. helped in the design of the experiments and the write-up of the manuscript. All authors have read and agreed to the published version of the manuscript.

**Funding:** Funding for this research was provided by NSERC.

**Conflicts of Interest:** The authors declare no conflict of interest.

## References

1. Brandrup, J.; Immergut, E.H.; Grulke, E.A. (Eds.) *In Polymer Handbook*, 4th ed.; Wiley: New York, NY, USA, 1999; pp. 1–83.
2. Lakowicz, J.R. *In Principles of Fluorescence Spectroscopy*, 3rd ed.; Springer: New York, NY, USA, 2006; pp. 277–330.
3. Duhamel, J. Global Analysis of Fluorescence Decays to Probe the Internal Dynamics of Fluorescently Labeled Macromolecules. *Langmuir* **2013**, *30*, 2307–2324. [[CrossRef](#)] [[PubMed](#)]
4. Duhamel, J. Internal Dynamics of Dendritic Molecules Probed by Pyrene Excimer Formation. *Polymers* **2012**, *4*, 211–239. [[CrossRef](#)]
5. Duhamel, J. New Insights in the Study of Pyrene Excimer Fluorescence to Characterize Macromolecules and their Supramolecular Assemblies in Solution. *Langmuir* **2012**, *28*, 6527–6538. [[CrossRef](#)]
6. Siu, H.; Duhamel, J. Comparison of the Association Level of a Hydrophobically Modified Associative Polymer Obtained from an Analysis Based on Two Different Models. *J. Phys. Chem. B* **2005**, *109*, 1770–1780. [[CrossRef](#)] [[PubMed](#)]
7. Birks, J.B. *Photophysics of Aromatic Molecules*; Wiley: London, UK, 1970.
8. Winnik, M.A. End-to-end cyclization of polymer chains. *Accounts Chem. Res.* **1985**, *18*, 73–79. [[CrossRef](#)]
9. Chen, S.; Duhamel, J.; Winnik, M.A. Probing End-to-End Cyclization Beyond Willemski and Fixmann. *J. Phys. Chem. B* **2011**, *115*, 3289–3302. [[CrossRef](#)]
10. Cuniberti, C.; Perico, A. Intramolecular excimer formation in polymers. *Eur. Polym. J.* **1980**, *16*, 887–893. [[CrossRef](#)]
11. Yip, J.; Duhamel, J.; Bahun, G.J.; Adronov, A. A Study of the Dynamics of the Branch Ends of a Series of Pyrene-Labeled Dendrimers Based on Pyrene Excimer Formation. *J. Phys. Chem. B* **2010**, *114*, 10254–10265. [[CrossRef](#)]
12. Modrakowski, C.; Flores, S.C.; Beinhoff, M.; Schlüter, A.D. Synthesis of Pyrene Containing Building Blocks for Dendrimer Synthesis. *Synthese* **2001**, *2001*, 2143–2155. [[CrossRef](#)]
13. Figueira-Duarte, T.M.; Simon, S.C.; Wagner, M.; Druzhinin, S.I.; Zachariasse, K.A.; Müllen, K. Polypyrene Dendrimers. *Angew. Chem. Int. Ed.* **2008**, *47*, 10175–10178. [[CrossRef](#)]
14. Figueira-Duarte, T.M.; Müllen, K. Pyrene-Based Materials for Organic Electronics. *Chem. Rev.* **2011**, *111*, 7260–7314. [[CrossRef](#)] [[PubMed](#)]
15. Stewart, G.M.; Fox, M.A. Fluorophore-labeled dendrons as light harvesting antennae. *J. Am. Chem. Soc.* **1996**, *118*, 4354–4360. [[CrossRef](#)]

16. Giovanella, U.; Mróz, W.; Foggi, P.; Fabbrizzi, P.; Cicchi, S.; Botta, C. Multi-Colour Electroluminescence of Dendronic Antennae Containing Pyrenes as Light Harvesters. *ChemPhysChem* **2009**, *11*, 683–688. [[CrossRef](#)] [[PubMed](#)]
17. Thomas, K.R.J.; Thompson, A.L.; Sivakumar, A.V.; Bardeen, C.J.; Thayumanavan, S. Energy and Electron Transfer in Bifunctional Non-Conjugated Dendrimers. *J. Am. Chem. Soc.* **2005**, *127*, 373–383. [[CrossRef](#)] [[PubMed](#)]
18. Vanjinathan, M.; Lin, H.-C.; Nasar, A.S. Synthesis, Characterization and Photophysical Properties of DCM-Based Light-Harvesting Dendrimers. *Macromol. Chem. Phys.* **2011**, *212*, 849–859. [[CrossRef](#)]
19. Gu, T.; Whitesell, J.K.; Fox, M.A. Intramolecular Charge Transfer in 1:1 Cu(II)/Pyrenylcyclam Dendrimer Complexes. *J. Phys. Chem. B* **2006**, *110*, 25149–25152. [[CrossRef](#)]
20. Morales-Espinoza, E.G.; Lijanova, I.V.; Morales-Saavedra, O.G.; Torres-Zuñiga, V.; Hernández-Ortega, S.; Garcia, M.M. Synthesis of Porphyrin-Dendrimers with a Pyrene in the Periphery and Their Cubic Nonlinear Optical Properties. *Molecules* **2011**, *16*, 6950–6968. [[CrossRef](#)]
21. Baker, L.A.; Crooks, R.M. Photophysical Properties of Pyrene-Functionalized Poly (propylene imine) Dendrimers. *Macromolecules* **2000**, *33*, 9034–9039. [[CrossRef](#)]
22. Wang, B.-B.; Zhang, X.; Jia, X.-R.; Li, Z.-C.; Ji, Y.; Yang, L.; Wei, Y. Fluorescence and aggregation behaviour of poly(amidoamine) dendrimers peripherally modified with aromatic fluorophores: The effect of dendritic architecture. *J. Am. Chem. Soc.* **2004**, *126*, 15180–15194. [[CrossRef](#)]
23. Wang, B.-B.; Zhang, X.; Yang, L.; Jia, X.-R.; Ji, Y.; Li, W.-S.; Wei, Y. Poly (amisoamine) dendrimers bearing electron-donating fluorophores: Fluorescence and electrochemical properties. *Polym. Bull.* **2006**, *56*, 63–74. [[CrossRef](#)]
24. Brauge, L.; Caminade, A.-M.; Majoral, J.-P.; Slomkowski, S.; Wolszczak, M. Segmental Mobility in Phosphorus-Containing Dendrimers. Studies by Fluorescent Spectroscopy. *Macromolecules* **2001**, *34*, 5599–5606. [[CrossRef](#)]
25. Brauge, L.; Veriot, G.; Franc, G.; Deloncle, R.; Caminade, A.-M.; Majoral, J.-P. Synthesis of phosphorus dendrimers bearing chromophoric end groups: Toward organic blue light-emitting diodes. *Tetrahedron* **2006**, *62*, 11891–11899. [[CrossRef](#)]
26. Caminade, A.-M.; Hameau, A.; Turrin, C.-O.; Ianchuk, M.; Delavaux-Nicot, B.; Majoral, J.-P. Fluorescent Phosphorus Dendrimers and Their Role in Supramolecular Interactions. *Phosphorus Sulfur Silicon Relat. Elem.* **2011**, *186*, 860–868. [[CrossRef](#)]
27. Lekha, P.K.; Prasad, E. Tunable Emission of Static Excimer in a Pyrene-Modified Polyamidoamine Dendrimer Aggregate through Positive Solvatochromism. *Chem. A Eur. J.* **2011**, *17*, 8609–8617. [[CrossRef](#)] [[PubMed](#)]
28. Wilken, R.; Adams, J. End-group dynamics of fluorescently labeled dendrimers. *Macromol. Rapid Commun.* **1997**, *18*, 659–665. [[CrossRef](#)]
29. McNelles, S.A.; Thoma, J.L.; Adronov, A.; Duhamel, J. Quantitative Characterization of the Molecular Dimensions of Flexible Dendritic Macromolecules in Solution by Pyrene Excimer Fluorescence. *Macromolecules* **2018**, *51*, 1586–1590. [[CrossRef](#)]
30. Press, W.H.; Flanery, B.P.; Tenkolsky, S.A.; Vetterling, W.T. *Numerical Recipes in Fortran: The Art of Scientific Computing*; Cambridge University Press: New York, NY, USA, 1992; pp. 523–528.
31. Farhangi, S.; Casier, R.; Li, L.; Thoma, J.L.; Duhamel, J. Characterization of the Long-Range Internal Dynamics of Pyrene-Labeled Macromolecules by Pyrene Excimer Fluorescence. *Macromolecules* **2016**, *49*, 9597–9604. [[CrossRef](#)]
32. Farhangi, S.; Duhamel, J. Long Range Polymer Chain Dynamics Studied by Fluorescence Quenching. *Macromolecules* **2016**, *49*, 6149–6162. [[CrossRef](#)]
33. Lide, D.R. *CRC Handbook of Chemistry and Physics*, 77th ed.; CRC Press: Boca Raton, FL, USA, 1996.
34. Hall, T.; Whitton, G.; Casier, R.; Gauthier, M.; Duhamel, J. Arborescent Poly(l-glutamic acid)s as Standards To Study the Dense Interior of Polypeptide Mesoglobules by Pyrene Excimer Fluorescence. *Macromolecules* **2018**, *51*, 7914–7923. [[CrossRef](#)]
35. Casier, R.; Duhamel, J. Effect of Like Charges on the Conformation and Internal Dynamics of Polypeptides Probed by Pyrene Excimer Fluorescence. *Macromolecules* **2020**, *53*, 5147–5157. [[CrossRef](#)]

**Publisher’s Note:** MDPI stays neutral with regard to jurisdictional claims in published maps and institutional affiliations.



© 2020 by the authors. Licensee MDPI, Basel, Switzerland. This article is an open access article distributed under the terms and conditions of the Creative Commons Attribution (CC BY) license (<http://creativecommons.org/licenses/by/4.0/>).